ELSEVIER

Science and Technology of Advanced Materials 4 (2003) 559–564

SCIENCE AND TECHNOLOGY OF ADVANCED MATERIALS

www.elsevier.com/locate/stam

Carbon system syntheses on a chip by multiple microplasma CVD

Tsuyohito Ito*, Ken Katahira, Azusa Asahara, Sergei A. Kulinich, Kazuo Terashima

Department of Advanced Materials Science, Graduate School of Frontier Sciences, The University of Tokyo, 5-1-5 Kashiwanoha, Kashiwa-shi, Chiba 277-8561, Japan

Received 4 September 2003; revised 24 September 2003; accepted 25 September 2003

Abstract

Different carbon nitride films are deposited in this study using a multiple DC microplasma chemical vapor deposition apparatus, a so-called plasma chip. Numerical evidence is obtained for the high deposition rate. It probably results from the high density of microplasma demonstrated with a simulation of DC microplasma by the particle-in-cell-Monte Carlo collision method. Moreover, we propose an RF apparatus with a carbon film matrix for improvement of disposability of electrodes of the DC apparatus.

Keywords: Microplasma; Plasma chip; Chemical vapor deposition; Carbon; Simulation

1. Introduction

Recently, microplasma has attracted much interest. Many studies have addressed the generation of microplasma, including microplasma generation with the scanning probe microscope technique [1], generation of microhollow cathode discharges [2], miniaturized inductively coupled plasma generation [3], microplasma generation with coplanar film electrodes (CFE) [4,5], and thermoelectron-enhanced microplasma generation [6].

From the viewpoint of material development, microplasma shows great promise because of its advantages. It has high density and is capable of being generated in a small space; it can also be obtained at low cost. For example, many high-density microplasmas can be generated in a small space simultaneously using a plasma chip [7,8]. Moreover, samples can be fabricated at a high deposition rate, which can be an advantage for material development. To date, we have confirmed the high density of the DC H_2 microplasma generated with CFE by optical emission spectroscopy (OES) [7]. In addition, carbon films were deposited with a prototype plasma chip [8].

This study presents carbon system syntheses on a chip by multiple microplasma chemical vapor depositions (CVD) using DC and RF apparatuses. First, different carbon nitride films are deposited using the multiple DC microplasma CVD apparatus. The high deposition rate was confirmed quantitatively. The high density of microplasma was confirmed by a computational method with 'NEPTUNE' software [9], which uses the particle-in-cell (PIC)-Monte Carlo collision (MCC) method [10,11], for a 10-μm-gap DC H_2 plasma previously observed by OES [7]. In addition to various plasma diagnostics, computational simulation methods might be useful for examining microplasma characteristics because experimental analyses of microplasma are difficult to perform because of its small scale. Next, because the electrodes were in a disposable state for only 2–3 min because of damage from the plasma for DC, an array of RF microplasmas and applying these RF plasmas for simultaneous processing with the same concept as a plasma chip were demonstrated.

2. Experimental

2.1. Multiple DC microplasma CVD: plasma chip

2.1.1. Carbon nitride film deposition

Carbon nitride films were deposited with a CH_4:N_2 gas system using a prototype plasma chip (Fig. 1) with 2×3 pairs of electrodes. Plasma was generated with DC power and 20-μm-gap platinum CFE. Gaseous ratios of N_2:CH_4 used were 5:1, 3:1 and 1:1. Total pressure was 600 Torr. The electric current was controlled at 1.0, 1.5, 2.0 and 2.5 μA.

* Corresponding author. Fax: +81-4-7136-3798.
E-mail address: ito@terra.mm.t.u-tokyo.ac.jp (T. Ito).

1468-6996/$ - see front matter © 2004 Elsevier Ltd. All rights reserved.
doi:10.1016/j.stam.2003.09.016

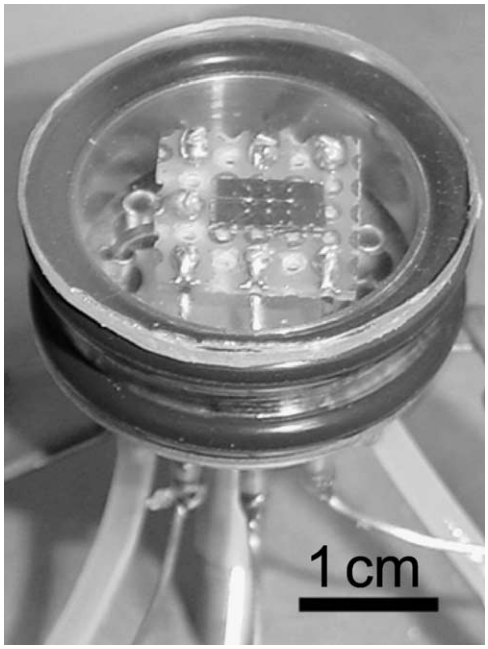

Fig. 1. Prototype plasma chip.

The platinum cathode was a substrate for deposition. Deposition time was about 60 s. The films deposited on platinum cathodes were characterized with Fourier transform infrared spectroscopy (FT-IR). A surface tracer showed mesoscopic surface morphologies for estimations of the deposition rate. Surface morphology was observed using an atomic force microscope (AFM).

2.1.2. Simulation of DC microplasma by PIC-MCC method

The high deposition rate of processing with a plasma chip might result from the high plasma density. We confirmed the high density by OES for 10-μm-gap DC H_2 microplasma [7], but the details of the plasma, such as potential distribution and electron and ion temperatures, remain unclear. Here we calculate not for the complex CH_4–N_2 plasma using in the processing, but for 10-μm-gap DC H_2 microplasma. The latter is simpler and can be compared with reported OES results. This simulation is based on a two-dimensional PIC-MCC method, which calculates the behavior of superparticles with a grid (cells) for field solving, such as potential. This simulation employs the MCC method of particle collision. Table 1 shows an outline of one step. This process is repeated until an equilibrium state is reached.

Table 1
Outline of one step in this simulation

Scatter and move	Calculations of velocities and positions of particles
Boundary adjustment	Calculations on boundaries, such as secondary electron emissions
MCC	Determination of kinds of collision and calculations of velocities of particles after collisions
Gather	Dividing electrical charges among grids
Field solve	Solving of potentials and electric fields

Table 2
Main parameters for H_2 microplasma simulation

Environmental condition	H_2, 760 Torr
Gap distance	10 μm
Cathode (left) condition	−350 V, $\gamma = 0.19$ ($T_i > 4.72$ eV)
Anode (right) condition	0 V

Table 2 lists calculation conditions, such as voltage and environmental pressure, depending on those previously reported [7]. Here, we calculated the microplasma generated with a DC bias voltage of 350 V in H_2 gas of 760 Torr pressure with electrodes 10 μm apart. The calculated field was 2×11 μm^2, which was separated to 4×22 by a grid for field solving. The upper and bottom boundaries without electrodes were simulated as periodic boundaries. The electrodes were located 10 μm apart and 0.5 μm from the left and right edges. The secondary emission coefficient (γ) on the cathode was set at 0.19 for an ion whose kinetic energy was more than 4.72 eV, which is one of the reported work functions for platinum. One superparticle was given the weight of 10^{12} cm^{-3}.

For H_2 plasma simulation, 14 reactions were considered. Table 3 shows those reactions, which include those of elastics, various excitations, ionizations, and charge exchange. Cross-sections for the MCC method were obtained from the literature [12,13]. A two-step ionization mechanism was not considered in these reactions. For ionization, only H_2^+ and H^+ ions created by electronic collisions with H_2 molecules were considered. The H_2^+ ionic transport was controlled by symmetric charge exchanges H_2^+/H_2. No reactions with H^+ were confirmed because the H^+ density was 1.5 orders lower than the H_2^+ density in our calculation. Therefore, in this simulation, calculations for electrons and H_2^+ ions were considered to be the most important and might be meaningful. Additionally, calculation results obtained from these reactions for macroscale plasma concurred well with previously reported results

Table 3
Considered reactions for H_2 microplasma simulation

$e + H_2 \rightarrow e + H_2$	Elastic
$e + H_2 \rightarrow e + H_2^*$	Rotational excitation $J = 0 \rightarrow 2$
$e + H_2 \rightarrow e + H_2^*$	Rotational excitation $J = 1 \rightarrow 3$
$e + H_2 \rightarrow e + H_2^*$	Vibrational excitation $V = 0 \rightarrow 1$–6
$e + H_2 \rightarrow e + H_2^*$	Electronic excitation $B^1\,\Sigma_u^+$
$e + H_2 \rightarrow e + H_2^*$	Electronic excitation $C^1\,\Pi_u$
$e + H_2 \rightarrow e + H_2^*$	Electronic excitation $b^3\,\Sigma_u^+$
$e + H_2 \rightarrow e + 2H^*$	Dissociative excitation Ly-α
$e + H_2 \rightarrow e + H + H^*$	Dissociative excitation H(2s)
$e + H_2 \rightarrow e + H + H^*$	Dissociative excitation Werner band
$e + H_2 \rightarrow e + H + H^*$	Dissociative excitation Lyman band
$e + H_2 \rightarrow 2e + H_2^+$	Ionization
$e + H_2 \rightarrow 2e + H + H^+$	Dissociative ionization
$H_2 + H_2^+ \rightarrow H_2^+ + H_2$	Symmetric charge exchange

calculated for electrons and H_2^+ ions. They were comparable to experimental results [14].

2.2. Development of multiple RF microplasma CVD apparatus

Fig. 2(a) shows a schematic diagram of the generators. It shows capacitive coupled-type plasma (CCP) generators arrayed to the *y* direction, which has different torch–sample distances (*z* direction), and a substrate that can be moved to the *x* direction. Glass tubes with 1 mm outer diameter and 0.5 mm inner diameter were used for tubes of torches; 100 μm diameter tungsten wires were used for inner electrodes. Torches and substrate were located in a plastic chamber. An RF power source (450 MHz, 30 W) was employed for simultaneous generations.

Carbon films were deposited on a nickel substrate using this apparatus with a CH_4 and Ar gas system. Environmental pressure was 760 Torr. The eight torch–substrate distances were slightly changed from 0.7 to 1.2 mm. The gaseous ratio of Ar to CH_4 was changed from 500:0.8 to 500:3.0. The total Ar flow rate was fixed at 500 ml/min. Respective deposition times were 3 min.

3. Results and discussion

3.1. Multiple DC microplasma CVD: plasma chip

3.1.1. Carbon nitride film deposition

Films deposited on the cathodes were characterized by FT-IR measurements as carbon nitride films. The films were amorphous, but the N content increased concomitant with increase in the gaseous ratio of N_2:CH_4. That change was detected by the change in the peak intensity ratio of N–H at around 3330 cm^{-1} to C–H at around 2950 cm^{-1}. Respective results and gas ratios for 1.5 μA were: 1.0 for 1:1 (N_2:CH_4), 2.5 for 3:1, and 2.8 for 5:1 (Fig. 3). Surface tracer measurements indicated the thickness distribution of the deposited films. As a typical example, the morphology for N_2:CH_4 = 3:1 with an electric current of 2.5 μA and a deposition time of 60 s (Fig. 4) indicates that the maximum thickness is 30–40 μm away from the gap, which was estimated to be 1.02 μm. Moreover, the films deposited on the anode and the damaged electrodes were confirmed. The maximum deposition rate increased with increased current, such as in the cases of the gaseous ratio of N_2:CH_4 = 3:1: 0.39 μm/min for 1.0 μA, 0.60 μm/min for 1.5 μA, 0.75 μm/min for 2.0 μA, and 1.02 μm/min for 2.5 μA. Figs. 5(a) and (b) show surface morphology of the film shown in Fig. 4 around the region with maximum film thickness (circle a in Fig. 4) and that of the platinum cathode used as the substrate. These images show that the film was deposited. The grain size was estimated to be about 0.2–0.5 μm with roughness of about 14 nm as a root mean square.

3.1.2. Simulation of DC microplasma by PIC-MCC method

Figs. 6 and 7 show calculated distributions of potential and the electron density between the electrodes (only the region between the electrodes is shown for simplicity). From these distributions, the bulk, 1.5 μm thick, located near the anode and the thickness of the cathode sheath, about 8 μm, are relatively large. They combine to more than one-half of the gap distance. The anode sheath is estimated to be about 0.5 μm thick. This structure agrees well with experimental observation by optical microscope. Figs. 8 and 9 show distributions of electron and H_2^+ ion energies, respectively. Fig. 8 shows electrons are accelerated (up to about 10^2 eV) in the cathode sheath; they

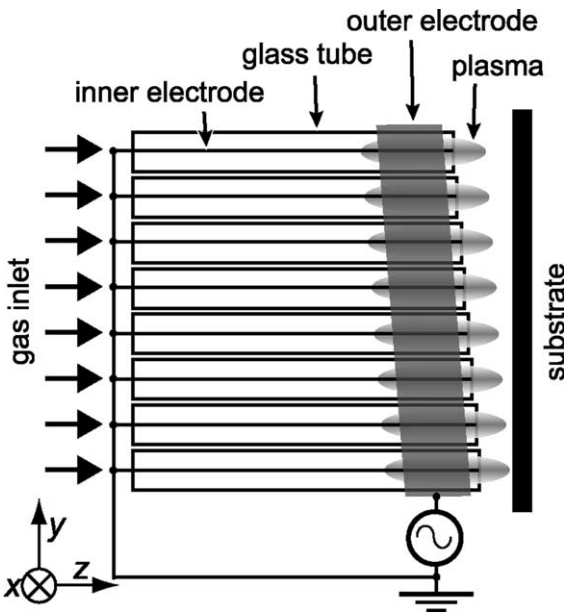

Fig. 2. Schematic diagram of multiple RF microplasma generators.

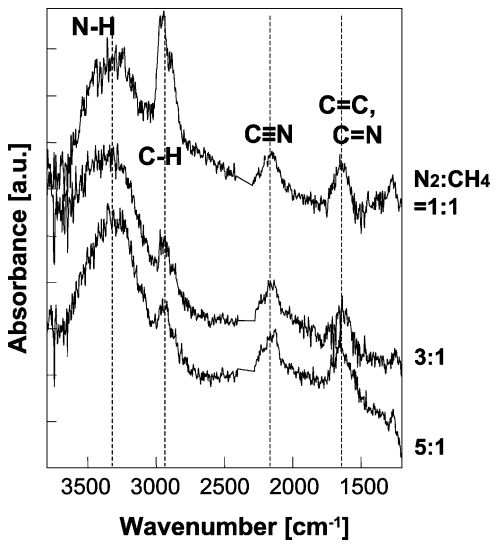

Fig. 3. Results of FT-IR measurements for the electric current of 1.5 μA.

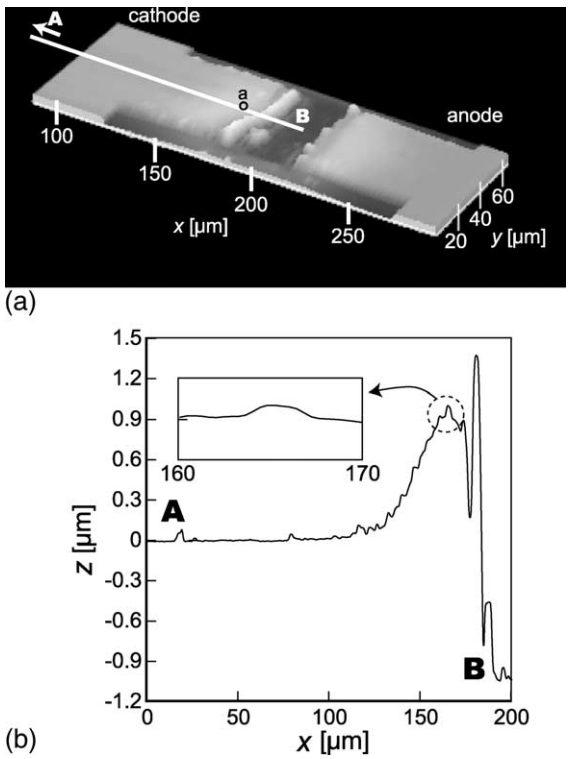

Fig. 4. Results of surface tracer measurement: x, distance; z, height. (a) Surface morphology near the gap. (b) Cross-section of the white line in (a). Level A is the cathode surface and B is the gap. The projection near $x = 180$ results from the damaged electrode.

yield excitation and ionization. Electron density, electron energy, and H_2^+ ion energy in the bulk (the region 0.5–2.0 μm away from the anode) are approximately 2.5–6.0 × 10^{21} m^{-3}, 0.3–3.0, and 0.06–0.20 eV, respectively. In addition, the electron density agrees with the reported value that was estimated using OES [7]. With an electron density of 5.5 × 10^{21} m^{-3} and an electron energy of 0.4 eV (with H_2^+ ion energy of 0.065 eV) at the center of the plasma, the Debye length λ_D is estimated to be ca. 0.065 μm, which is much smaller than the length of the plasma region (L), 1.5 μm. Also, the ion energy was found to be much lower than the electron energy. Therefore, this plasma is a high-density nonequilibrium plasma with a relatively large cathode sheath. Such high microplasma density, not only for this H_2 microplasma, might result from the highly dense (760 Torr) environment because the ionization coefficient is about 10^{-4}. That value is on the same order as the conventional macroscale.

3.2. Development of multiple RF microplasma CVD apparatus

Eight CCPs were generated simultaneously, as shown in Fig. 10. The plasma was very stable, with a duration time greater than one hour. That time is much longer than the duration time of DC microplasma with CFE of a few

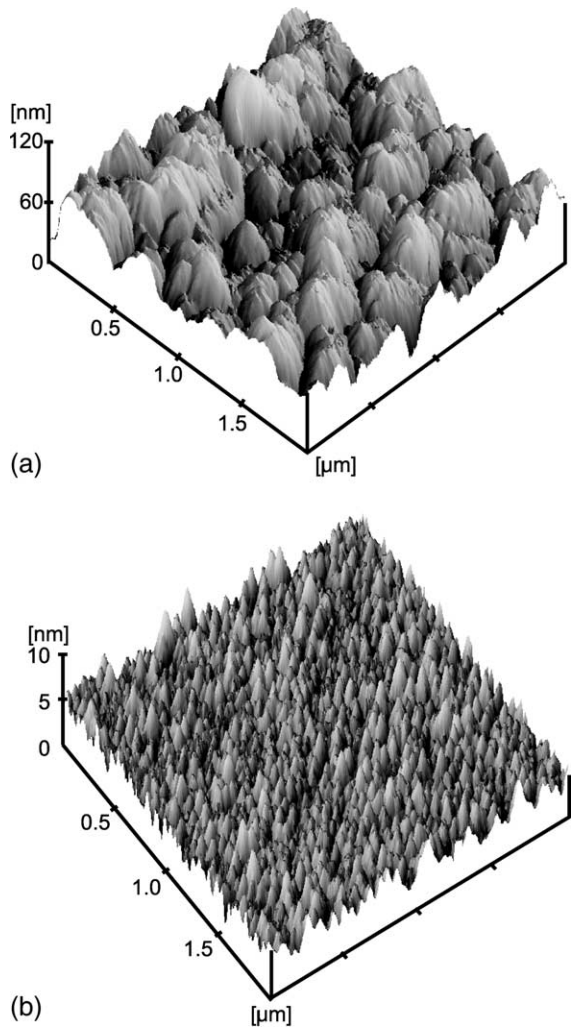

Fig. 5. (a) Surface morphology of a deposited film around the maximum film thickness region (circle a in Fig. 4(a)) measured by AFM. (b) Surface morphology of the platinum cathode that was used as the substrate.

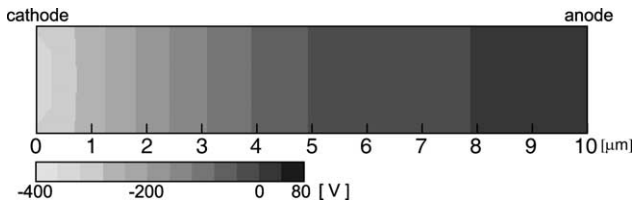

Fig. 6. Distribution of potential (10 μm gap, H_2 760 Torr, 350 V). Potentials of the cathode and anode are −350 and 0 V, respectively.

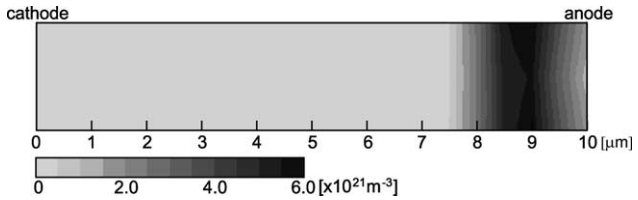

Fig. 7. Distribution of electron density (10 μm gap, H_2 760 Torr, 350 V).

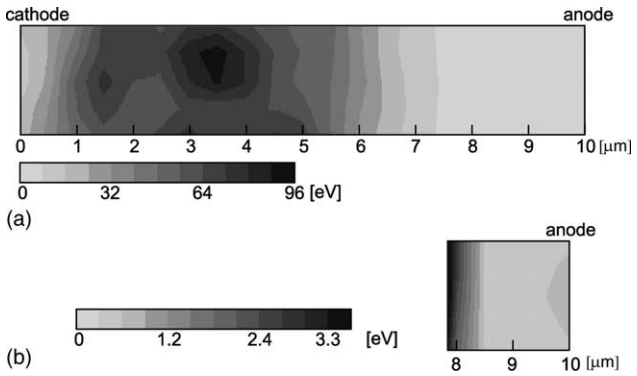

Fig. 8. Distributions of electron energy (10 μm gap, H_2 760 Torr, 350 V). (a) $x = 0–10$ μm, (b) $x \approx 8–10$ μm.

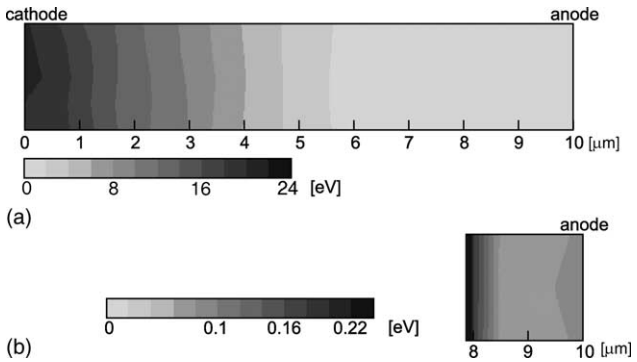

Fig. 9. Distributions of H_2^+ ion energy (10 μm gap, H_2 760 Torr, 350 V). (a) $x = 0–10$ μm, (b) $x \approx 8–10$ μm.

minutes [5]. Moreover, this apparatus is not disposable: many experimental series can be performed by changing substrates. Fig. 11 shows one example of a nickel substrate after a series of six processing cycles. Energy dispersive spectrometer measurements indicate that the deposited films (shown as circle shapes) are carbon films. No marked structural differences have been identified between the films, depending on deposition conditions of torch–substrate distances and gaseous ratios. However, we

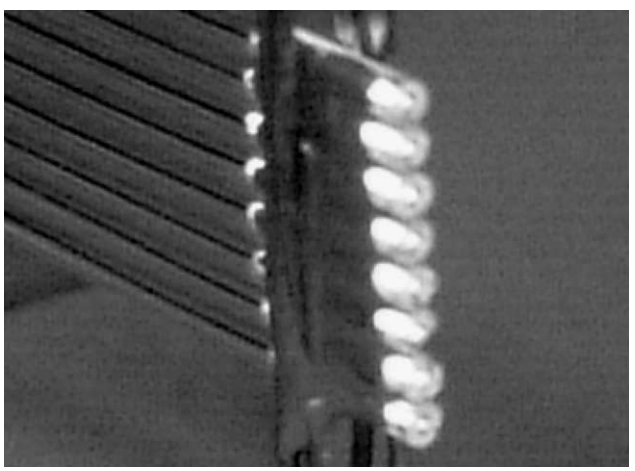

Fig. 10. Simultaneous generation of RF microplasmas.

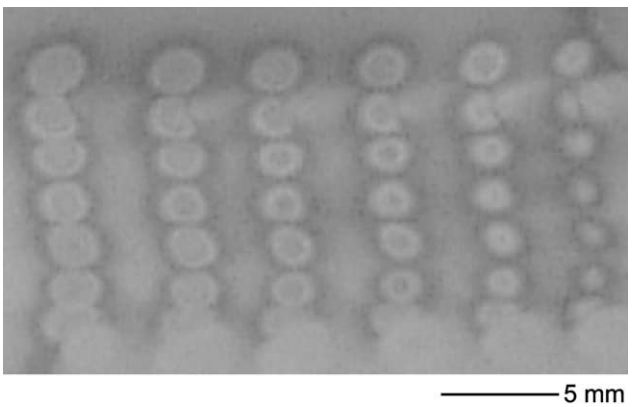

Fig. 11. Nickel substrate after depositions with total Ar flow of 500 ml/min and total CH_4 flows (from left-hand side) of 0.8, 1.1, 1.5, 1.9, 2.2 and 3.0 ml/min.

obtained a matrix of samples on one chip (substrate) with very stable RF microplasmas.

4. Conclusions

Different carbon nitride films were deposited successfully at a high deposition rate using a prototype plasma chip. It was confirmed quantitatively to be about 1 μm/min in the maximum case in this study. We inferred that the high deposition rate results from the high microplasma density. Characterization by computer simulation using the PIC-MCC method was performed for microplasma that was generated with a DC bias voltage of 350 V in H_2 gas of 760 Torr pressure with electrodes 10 μm apart. These results demonstrate that the plasma generated is a nonequilibrium high-density plasma with an electron density higher than 10^{21} m^{-3}. Results were confirmed experimentally and computationally. The cathode sheath is relatively thick. Moreover, a multiple RF microplasma CVD apparatus was developed: it improves duration time while providing multiple stable operations. Its high processing rate and possible simultaneous processing lead us to anticipate successful development of numerous materials with these microplasma CVD devices. Processing by these devices will engender deeper understanding through simulation methods: they will become an effective means for elucidating microplasma details.

Acknowledgements

The authors are extremely grateful to Professor Toyonobu Yoshida for his discussion and encouragement. We also thank Mr. Masaaki Tanaka (PEGASUS Software, Inc.) and Dr Eiichi Suetomi (CRC Corp.) for their great support in simulation. This work was supported in part by Grants-in-Aid for the Research Fellowship for Young

Scientists to T. I. from the Japan Society for the Promotion of Science.

References

[1] K. Terashima, L. Howald, H. Haefke, H. Güntherodt, Thin Solid Films 282 (1996) 634–636.
[2] K.H. Schoenbach, R. Verhappen, T. Tessnow, W.W. Byszewski, Appl. Phys. Lett. 68 (1996) 13–15.
[3] J. Hopwood, O. Minayeva, Y. Yin, J. Vac. Sci. Technol. B 18 (2000) 2446–2451.
[4] T. Ito, T. Izaki, K. Terashima, in: M. Hrabovský (Ed.), Proceedings of the 14th International Symposium on Plasma Chemistry (ISPC-14), Prague, 1999, pp. 967–972.
[5] T. Ito, T. Izaki, K. Terashima, Thin Solid Films 386 (2001) 300–304.
[6] T. Ito, K. Terashima, Appl. Phys. Lett. 80 (2002) 2648–2650.
[7] T. Ito, T. Izaki, K. Terashima, Surf. Coat. Technol. 133 (2000) 497–500.
[8] T. Ito, K. Terashima, Thin Solid Films 390 (2001) 234–236.
[9] CRC Solutions Corp.; upgraded to 'PEGASUS' (PEGASUS Software, Inc.).
[10] C.K. Birdsall, IEEE Trans. Plasma Sci. PS-19 (1991) 65–85.
[11] V. Vahedi, G. DiPeso, C.K. Birdsall, M.A. Lieberman, T.D. Rognlien, Plasma Sources Sci. Technol. 2 (1993) 261–272.
[12] T. Tawara, Y. Itikawa, H. Nishimura, M. Yoshino, J. Phys. Chem. Ref. Data 19 (1990) 617–636.
[13] A.V. Phelps, J. Phys. Chem. Ref. Data 19 (1990) 653–675.
[14] O. Leroy, P. Stratil, J. Perrin, J. Jolly, P. Belenguer, J. Phys. D 28 (1995) 500–507.